Supplement of Atmos. Chem. Phys., 25, 15033–15045, 2025 https://doi.org/10.5194/acp-25-15033-2025-supplement © Author(s) 2025. CC BY 4.0 License.





Supplement of

Emulating chemistry-climate dynamics with a linear inverse model

Eric J. Mei et al.

Correspondence to: Eric J. Mei (emei@uw.edu)

The copyright of individual parts of the supplement might differ from the article licence.

S1 Sensitivity of noise forcing to EOFs retained

Figure S1 shows the sensitivity of the negative eigenvalues in the noise forcing covariance **Q** to the number of EOFs used during calibration. The number of negative eigenvalues increase as more EOFs are added. The rescaling of the positive eigenvalues necessary also increases, though similar to the findings of Perkins and Hakim (2021), the rescaling is extremely sensitive to certain eigenvalues with no discernible trend.

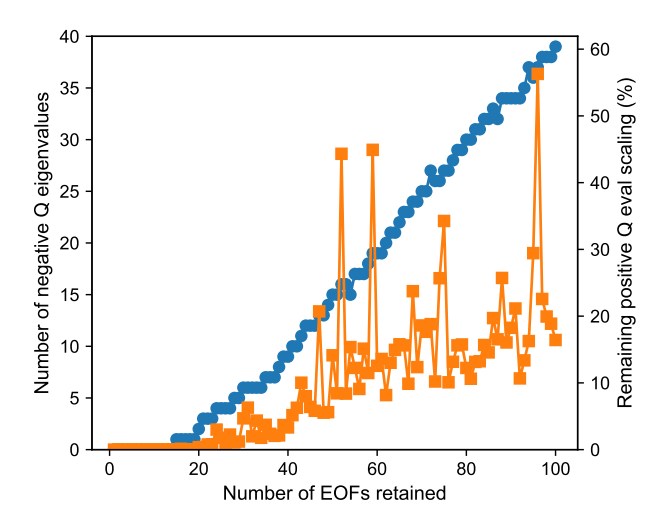


Figure S1: Sensitivity of negative eigenvalues in noise forcing covariance \mathbf{Q} to number of EOFs retained per variable in the SST-OH-O₃-NO_x-CO LIM. Number of negative eigenvalues (blue) and negative percentage of the total trace of \mathbf{Q} (orange) for a LIM calibrated on 2,000 years of monthly data.

S2 Results for variables not shown in the main text

Here, we show results of Figure 1 (Figure S2), Figure 3 (Figure S3), and Figure 4 (Figure S4) with nitrogen oxides (NO_x) and carbon monoxide (CO), which are not shown in the main text. Versions of Figure 5 with non-OH variables (SST, ozone, NO_x , and CO) are also shown (Figure S5 to Figure S8).

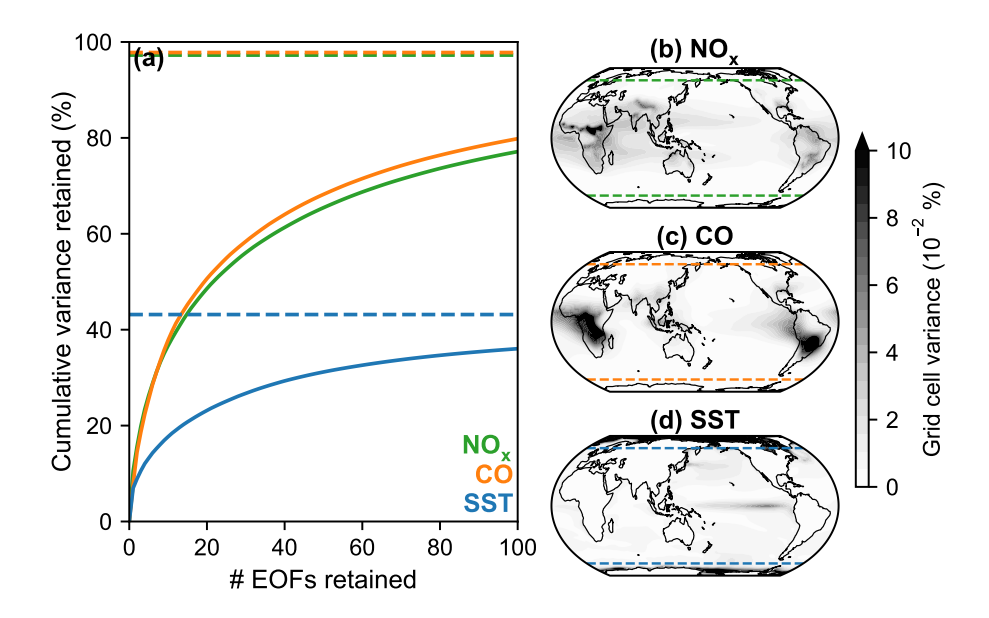


Figure S2: Same as Figure 2 in the main text but with NO_x and CO. Variance remaining after latitude masking and EOF truncation. (a) Cumulative percentage of global field variance retained as a function of the number of EOFs in the LIM state vector. Dashed lines indicate percentage of global field variance remaining after high latitudes are masked out. Percentage of global field variance in each grid cell for (b) NO_x , (c) CO, and (d) SST. Dashed lines indicate latitude cut-off for the high latitude mask.

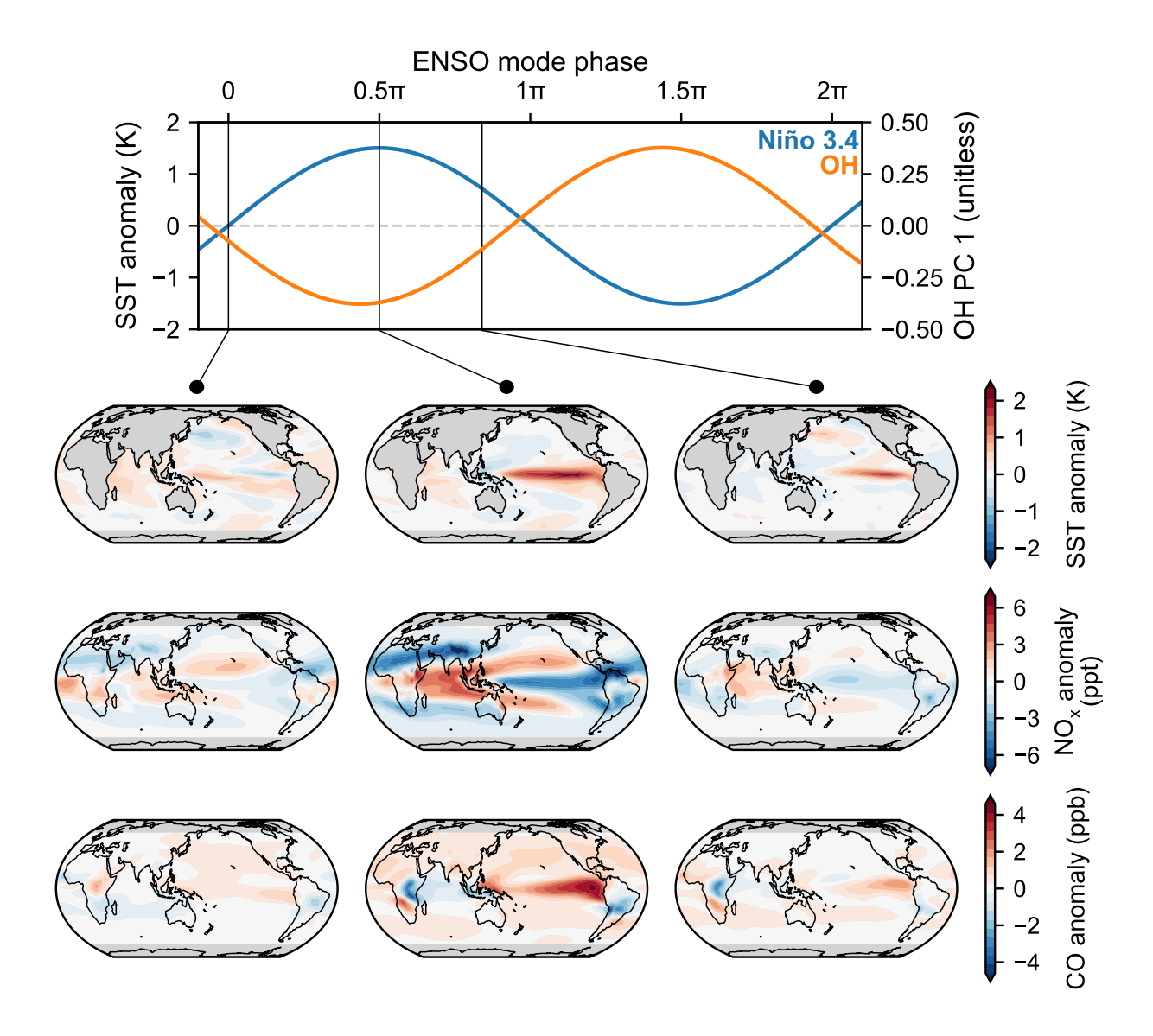


Figure S3: Same as Figure 3 in the main text but with NO_x and CO. Evolution of the oscillatory component of the ENSO mode without damping. (top) Timeseries of the Niño 3.4 index (blue) and the first principal component of OH (orange) as a function of phase. Three vertical black lines indicate three phases during the El Niño stage of the ENSO mode that are visualized in contour plots (bottom). From left to right, the columns of contour plots show snapshots of the growth, peak, and decay of anomalies in the phases of the ENSO mode. From top to bottom, the rows of contour plots show SST, NO_x , and CO anomalies.

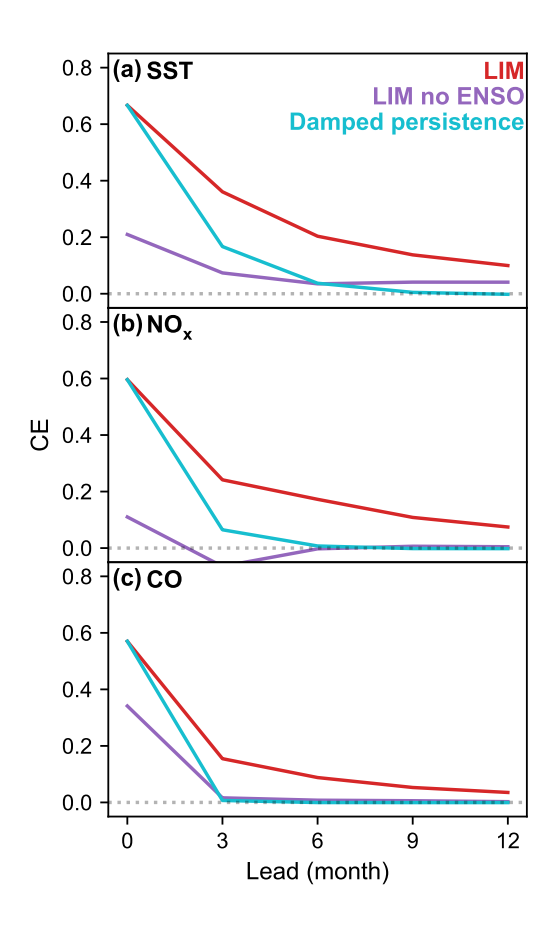


Figure S4: Same as Figure 4 in the main text but with NO_x and CO. Domain-averaged forecast skill (CE) over lead time from the LIM (red), the LIM with no ENSO mode (purple), and damped persistence (cyan) for (a) SST, (b) NO_x , and (c) CO. Dotted horizontal line indicates CE of climatology (CE=0).

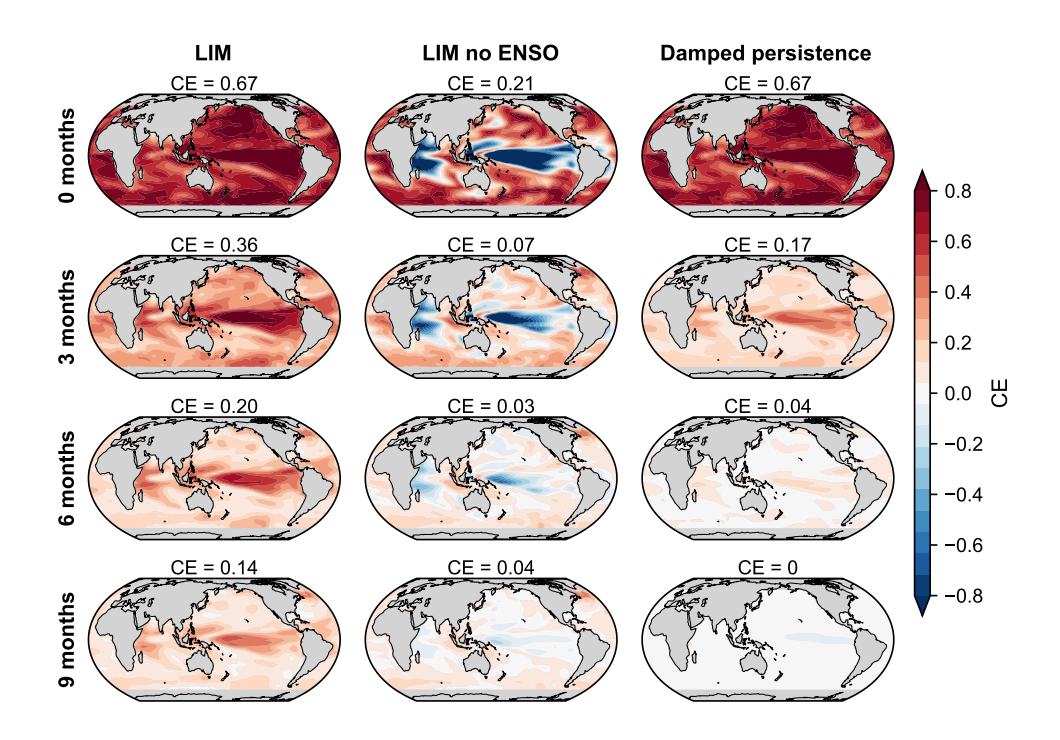


Figure S5: Same as Figure 4 in the main text but with SST. SST forecast skill (CE) over lead time from the LIM (*left column*), the LIM with no ENSO mode (*middle column*), and damped persistence (*right column*). Lead time increases from 0 months (*top row*) to 9 months (*bottom row*).

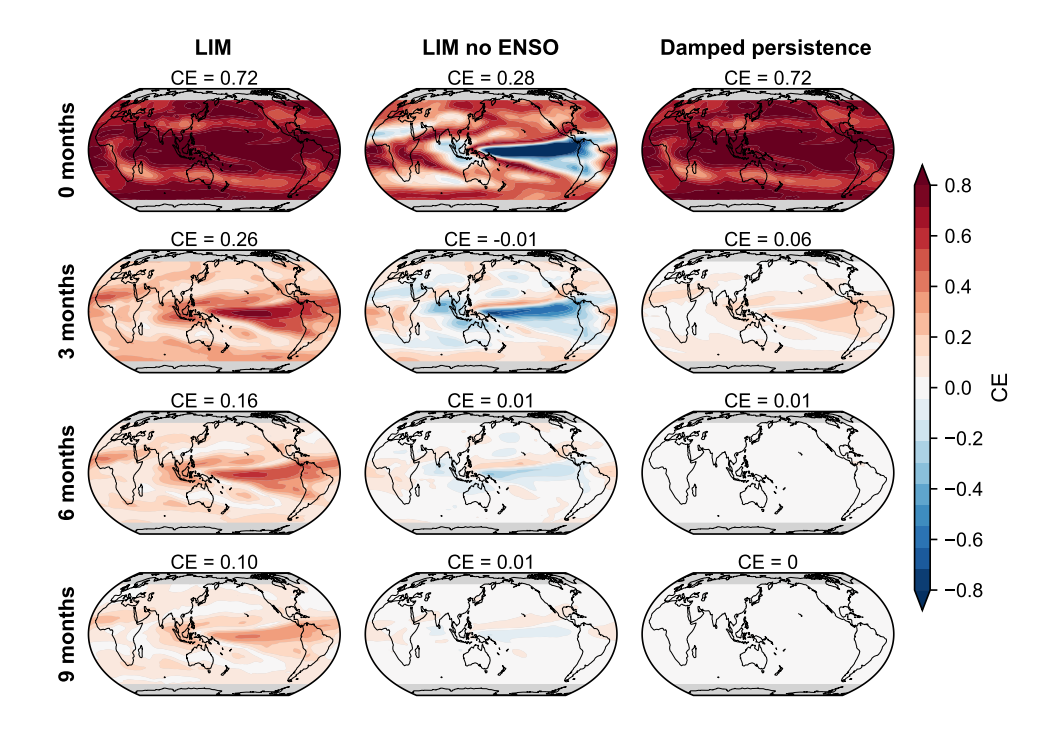


Figure S6: Same as Figure S5 but with ozone.

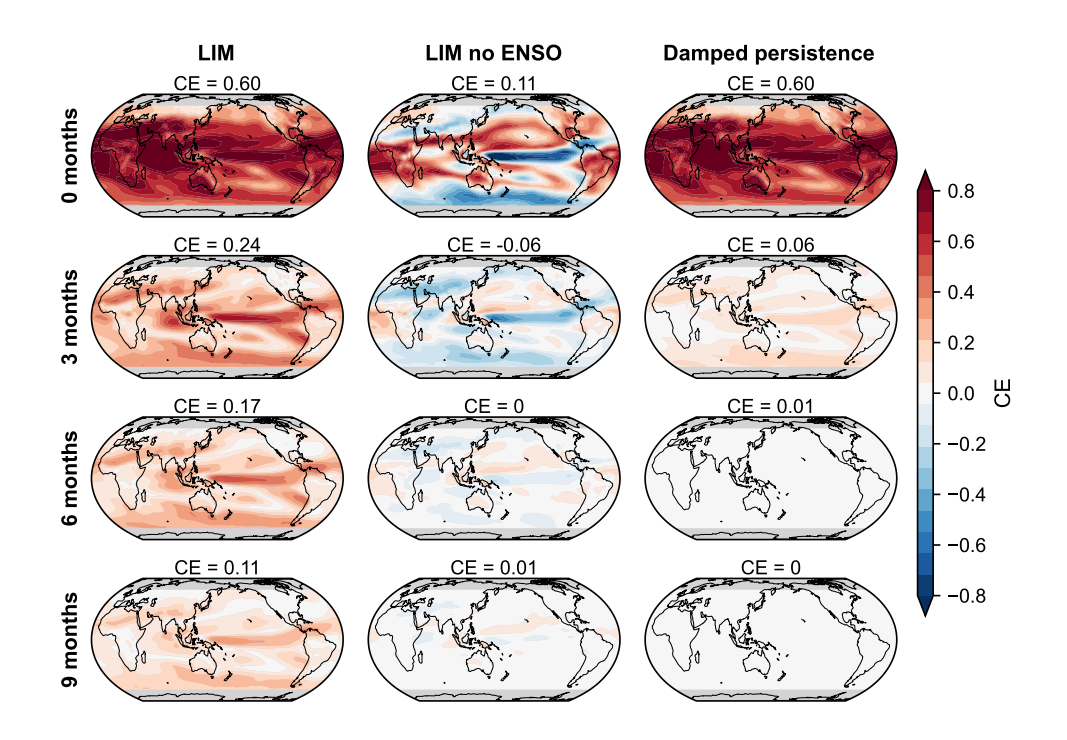


Figure S7: Same as Figure S5 but with NO_x .

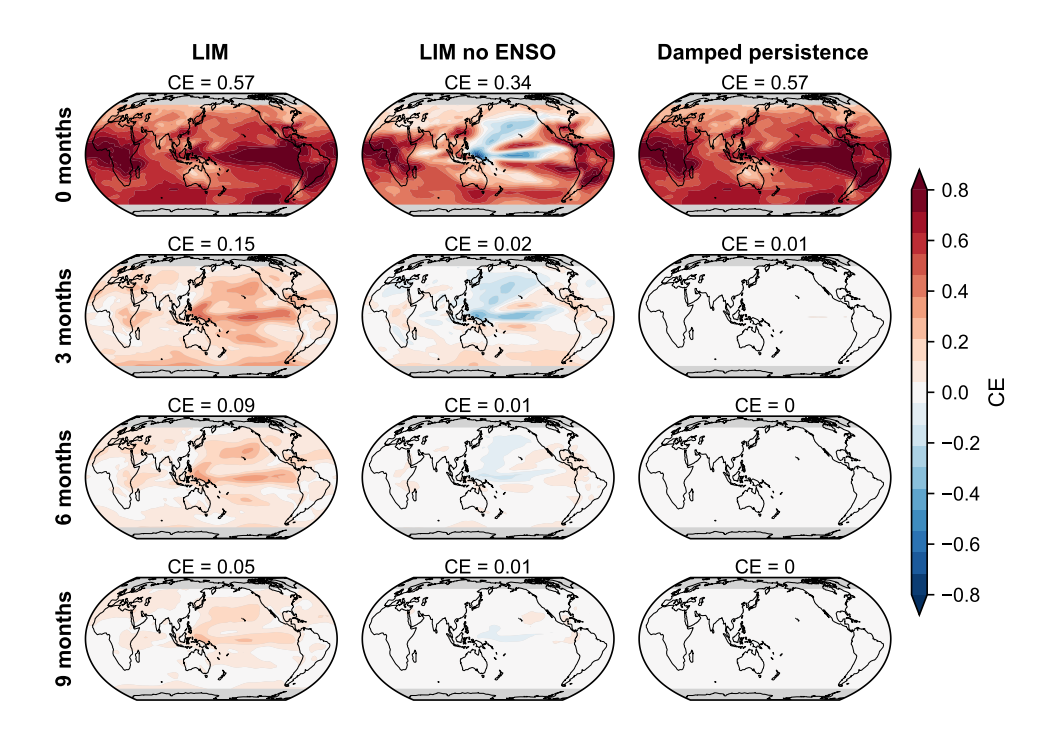


Figure S8: Same as Figure S5 but with CO.

S3 Forecast test results with correlation and RMSE

Here, we show results of Figure 4 and Figure 5 in the main text but with Pearson correlation (Figure S9, Figure S11 to Figure S15) and root mean square error (RMSE; Figure S10, Figure S16 to Figure S20)) instead of the coefficient of efficiency (CE).

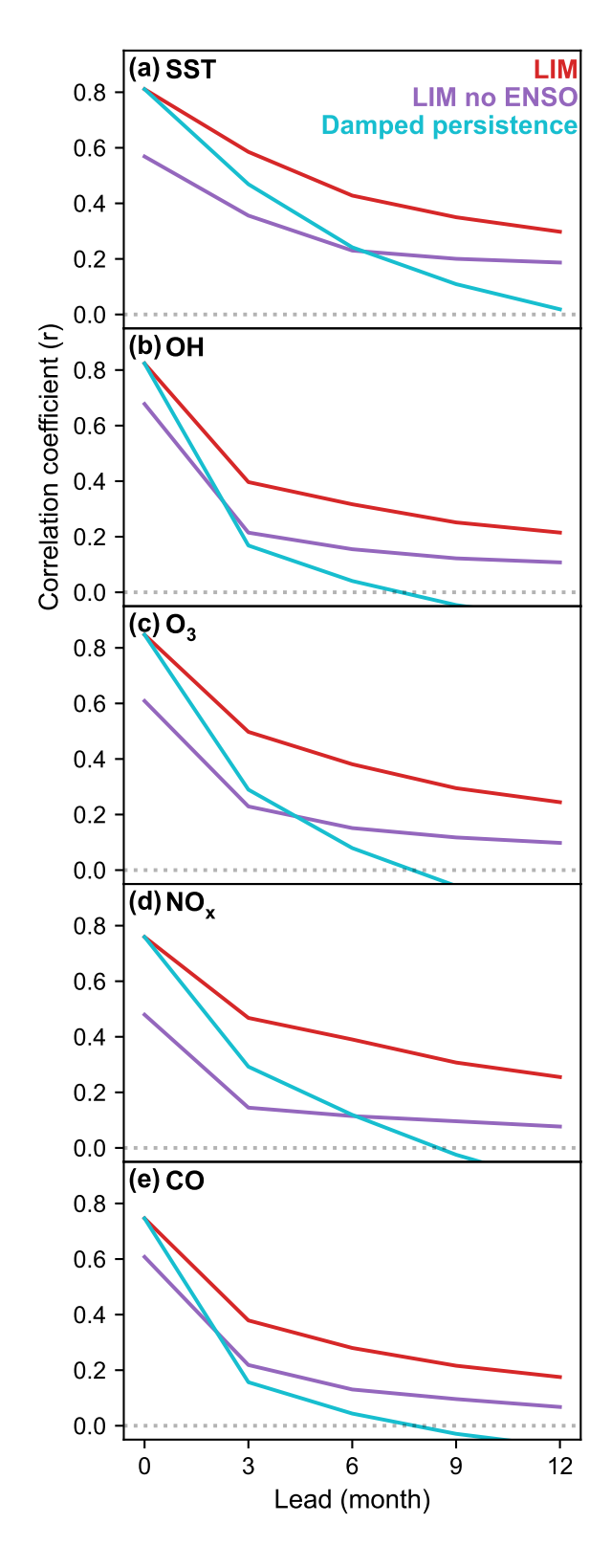


Figure S9: Same as Figure 4 in the main text but with the Pearson correlation instead of CE and with (d) NO_x and (e) CO.

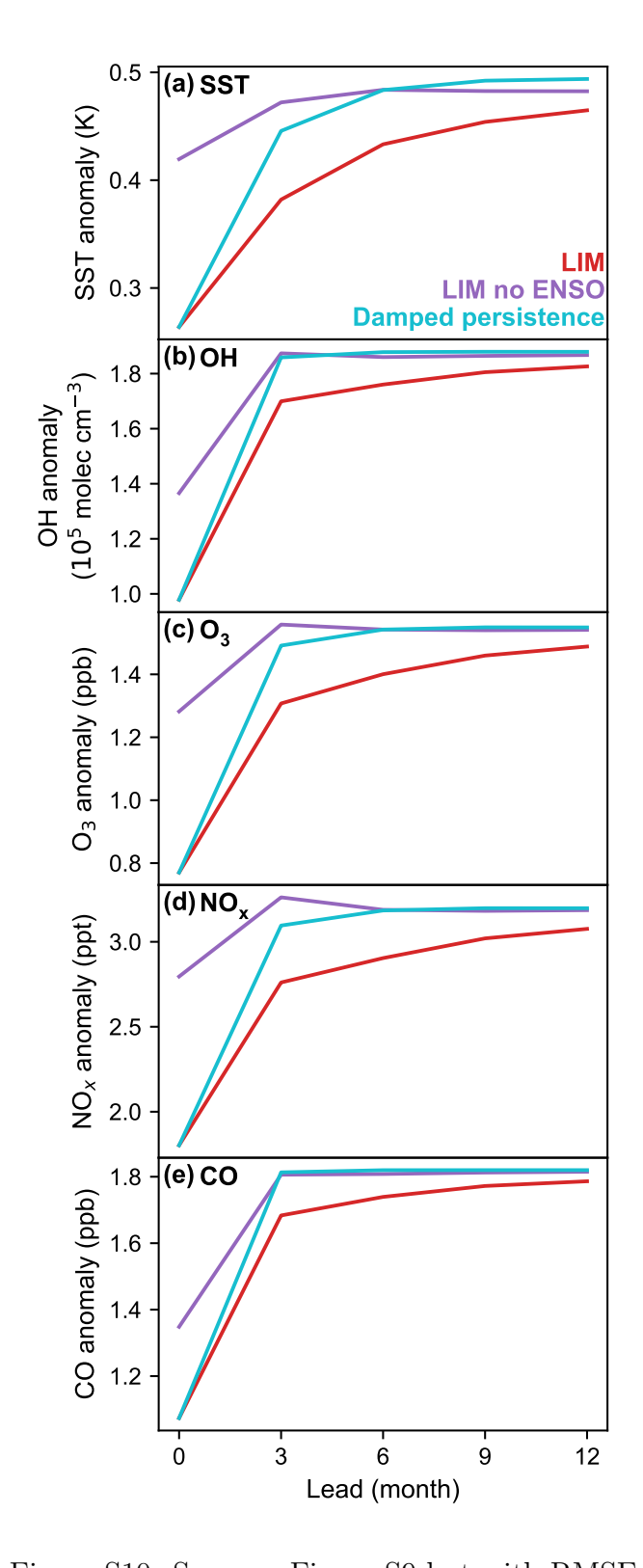


Figure S10: Same as Figure S9 but with RMSE.

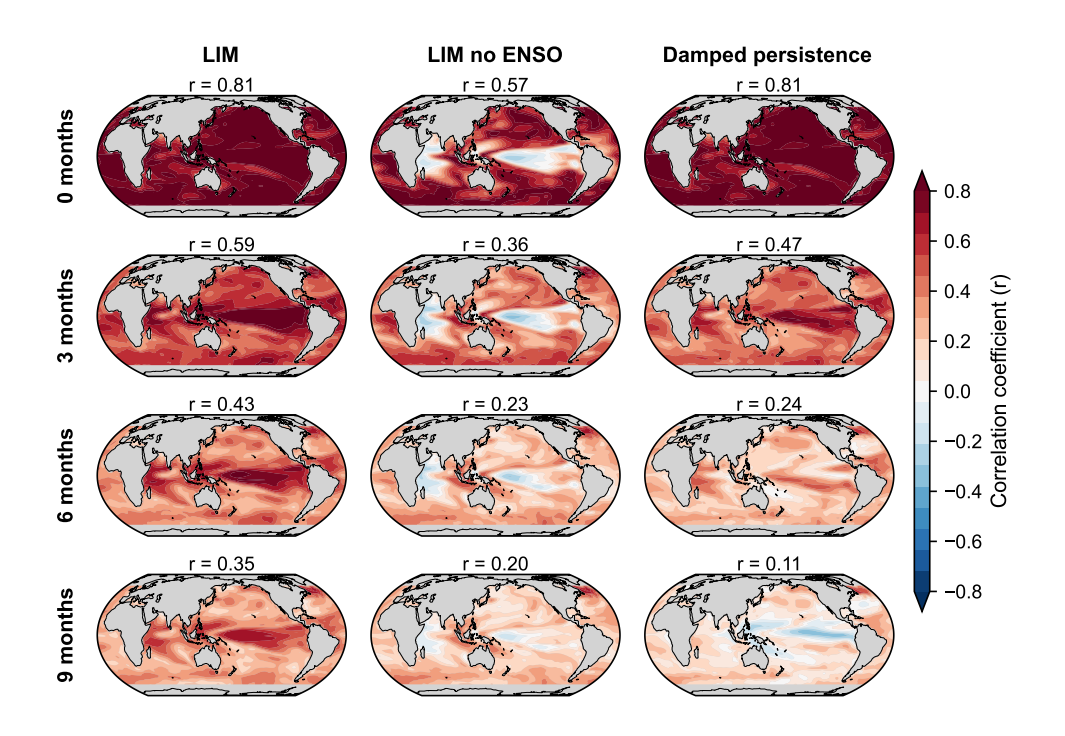


Figure S11: Same as Figure S5 but with Pearson correlation (r).

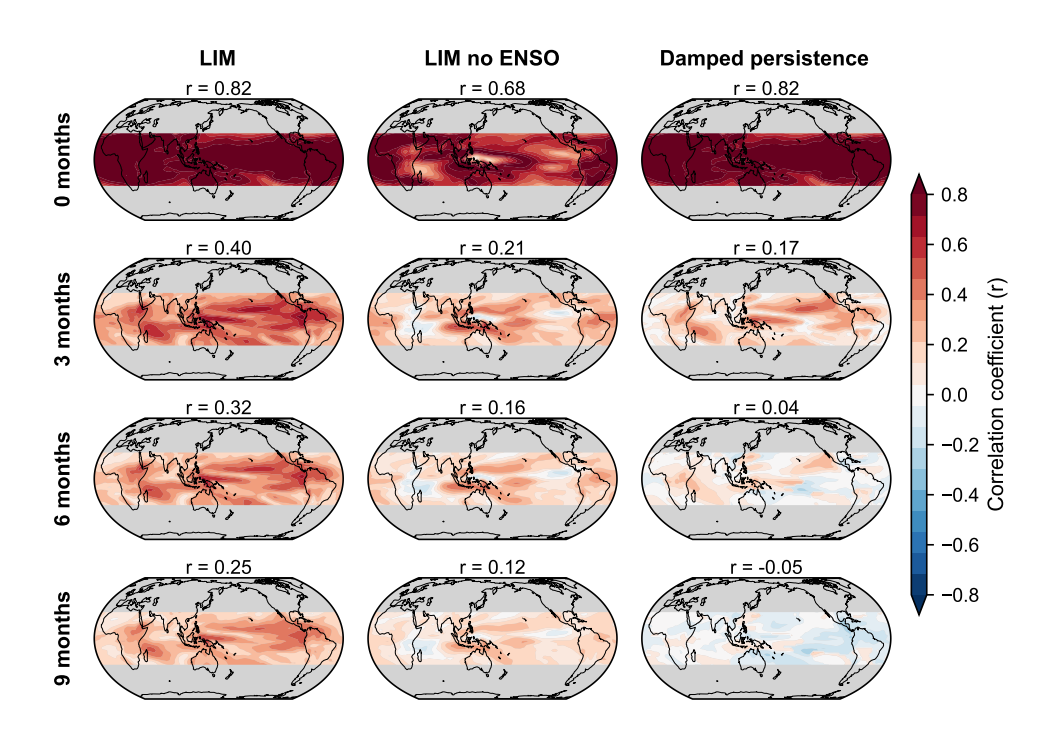


Figure S12: Same as Figure S11 but with OH.

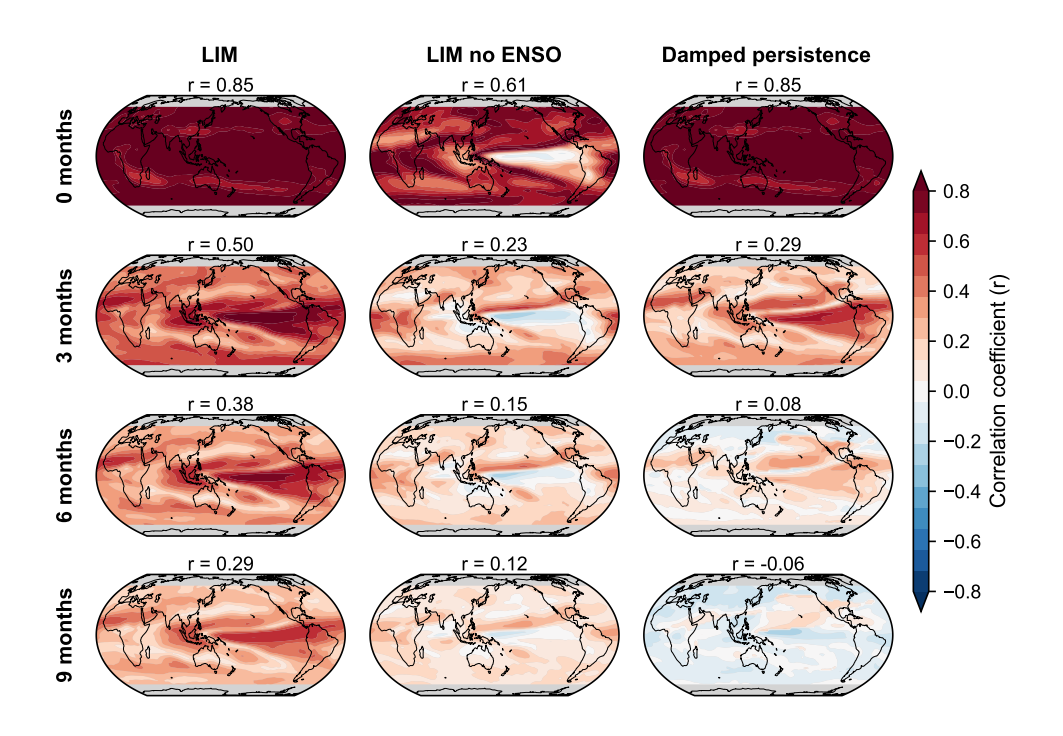


Figure S13: Same as Figure S11 but with ozone.

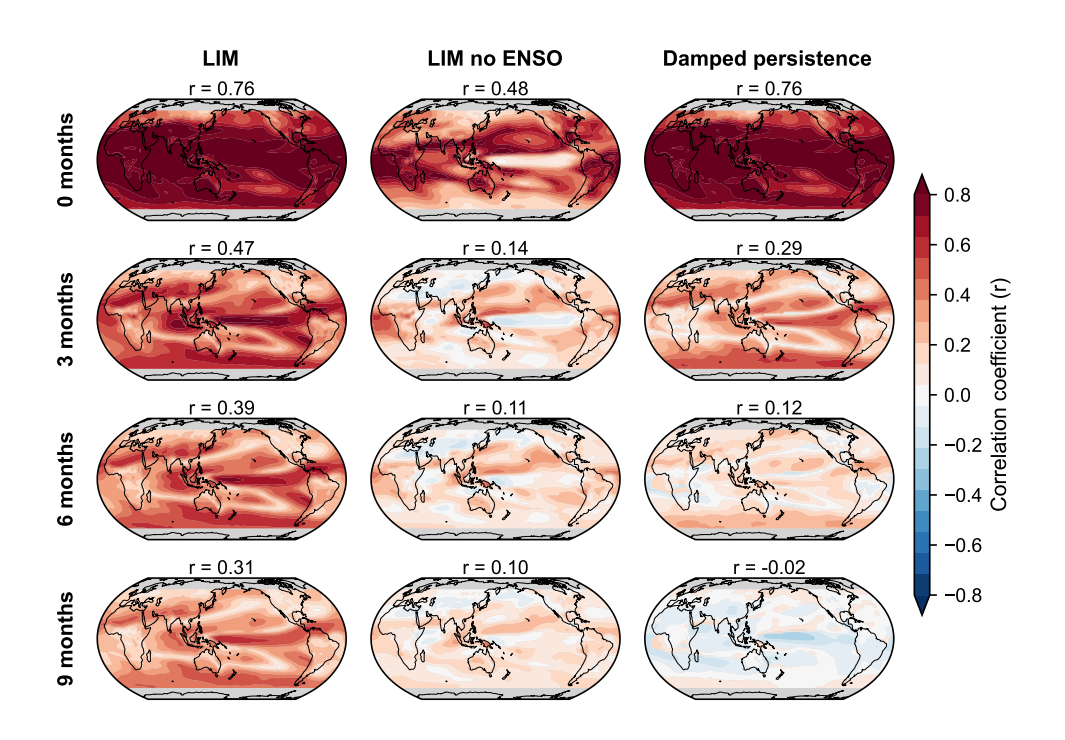


Figure S14: Same as Figure S11 but with NO_x .

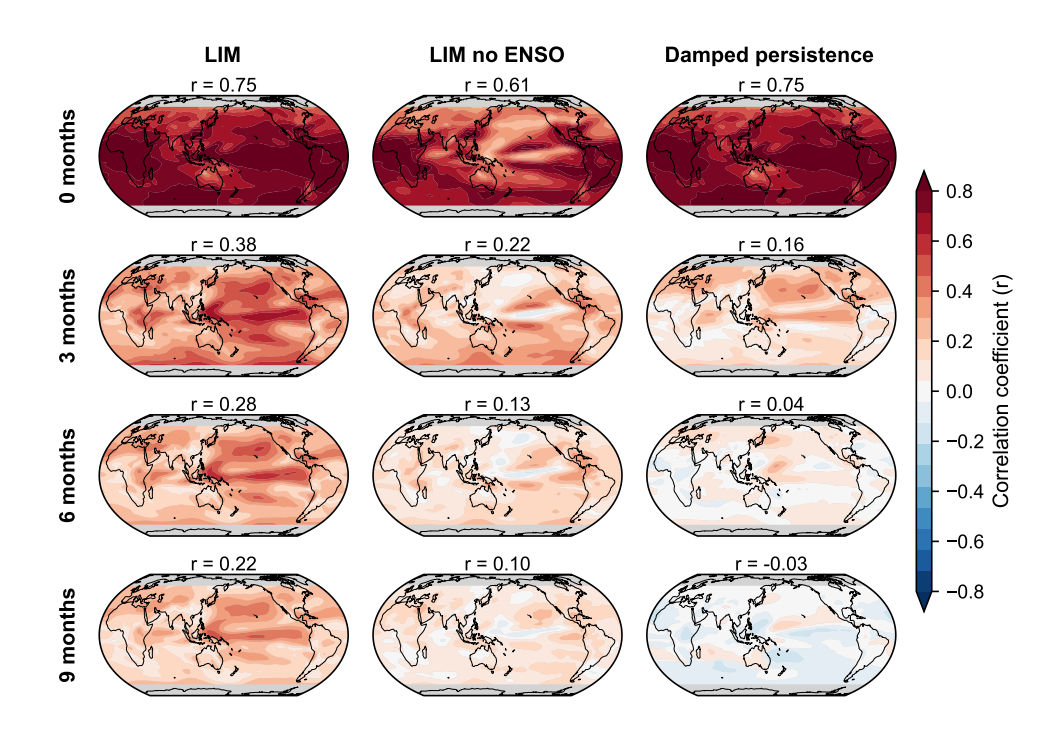


Figure S15: Same as Figure S11 but with CO.

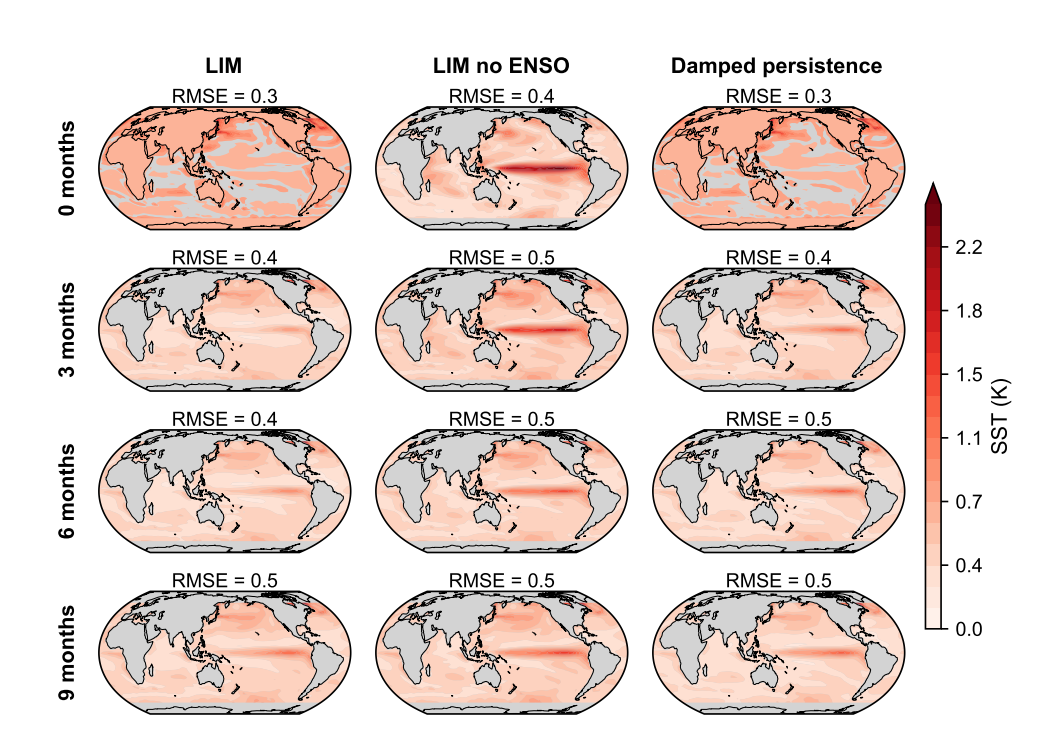


Figure S16: Same as Figure S5 but with RMSE.

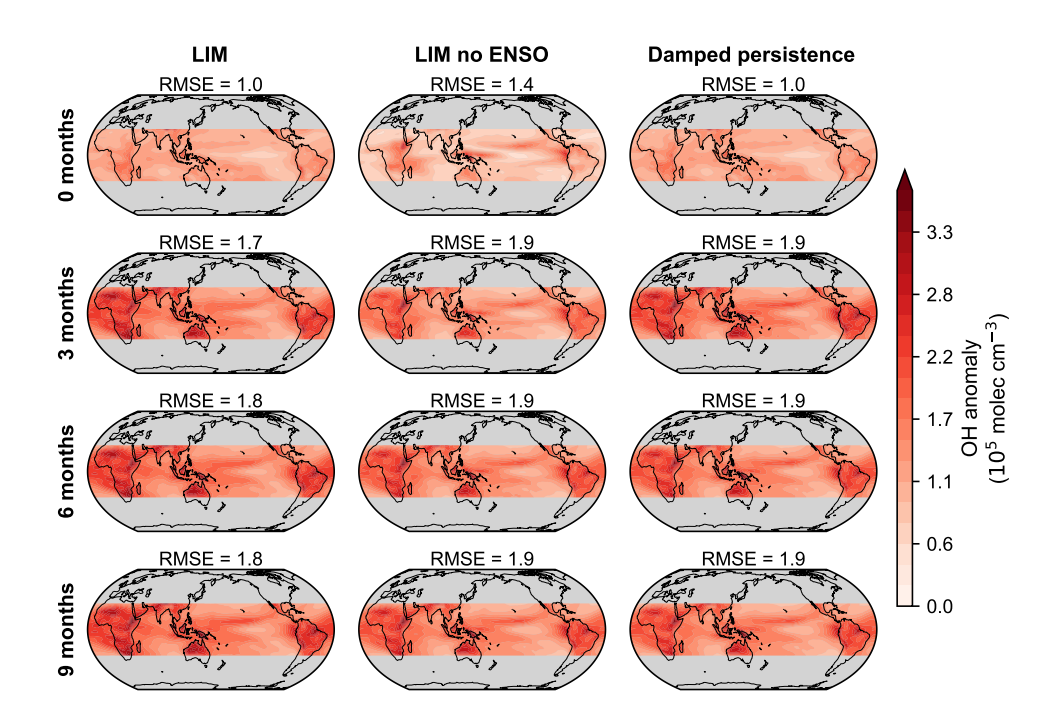


Figure S17: Same as Figure S16 but with OH.

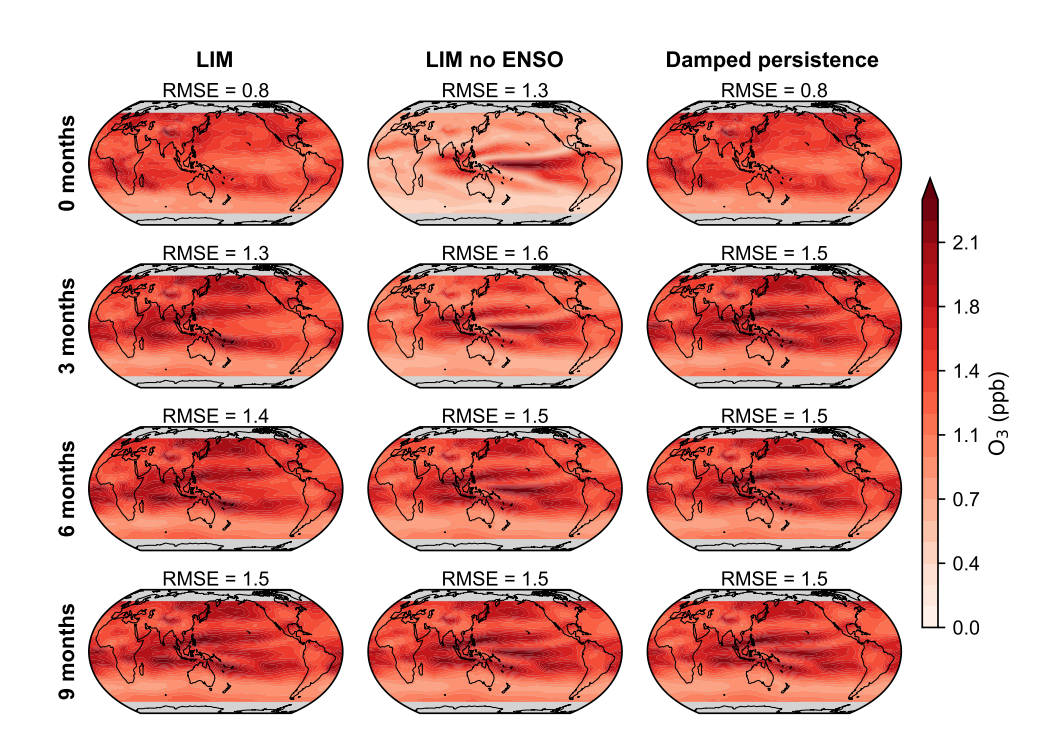


Figure S18: Same as Figure S16 but with ozone.

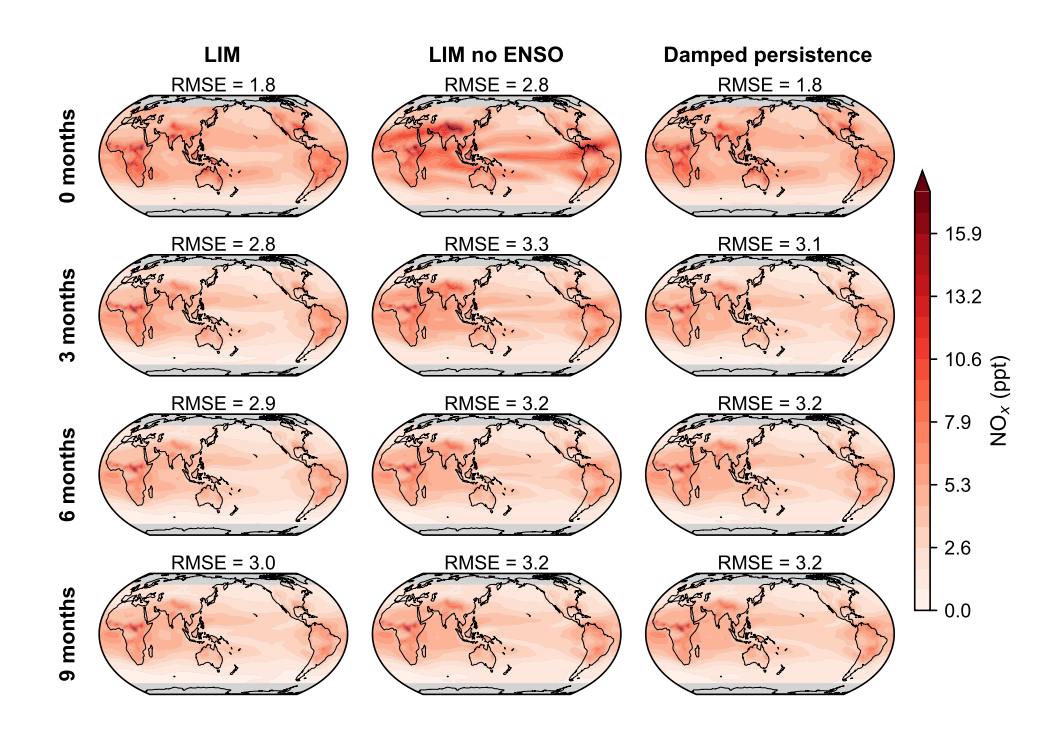


Figure S19: Same as Figure S16 but with NO_x .

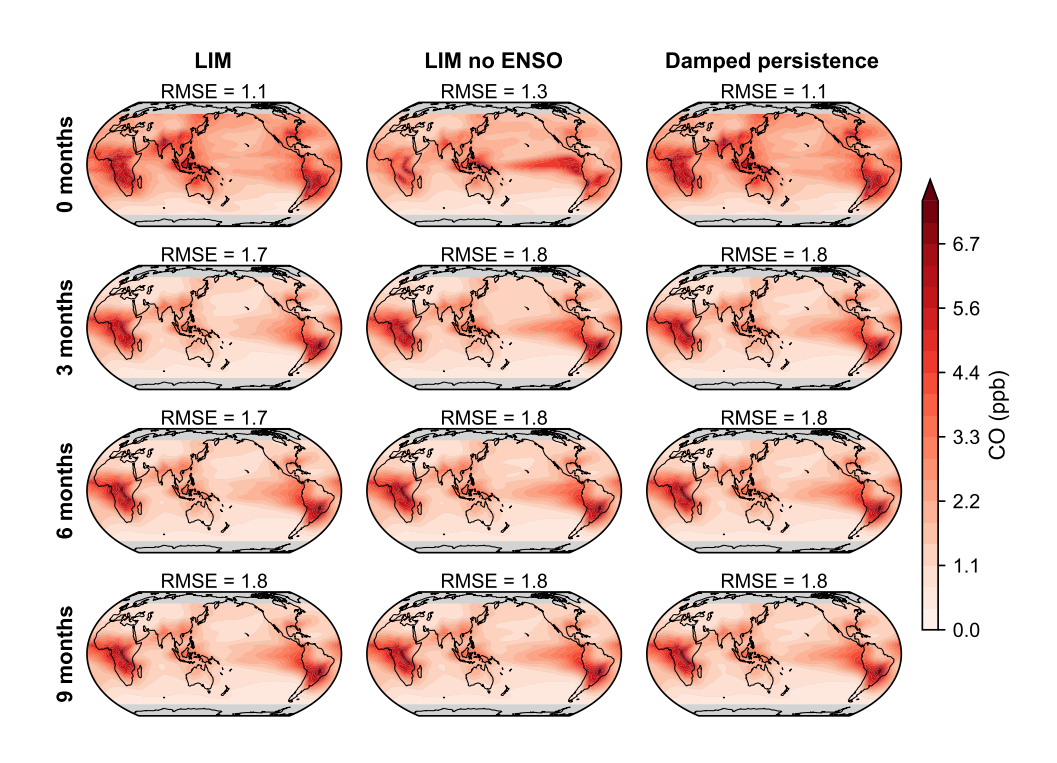


Figure S20: Same as Figure S16 but with CO.

S4 Chemistry-only LIM

Figure S21 to Figure S23 show the results of the forecast test with the chemistry-only LIM (OH, ozone, NO_x , CO).

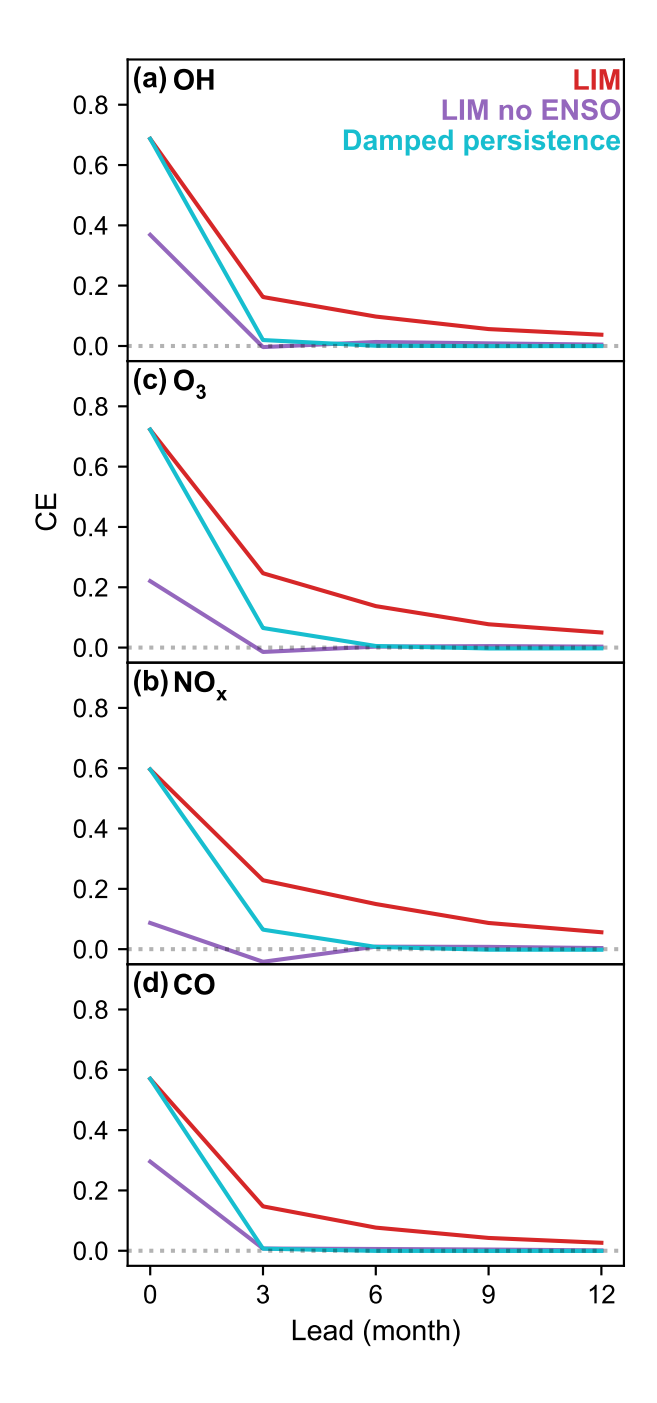


Figure S21: Same as Figure S9 but with the CE of the chemistry-only LIM.

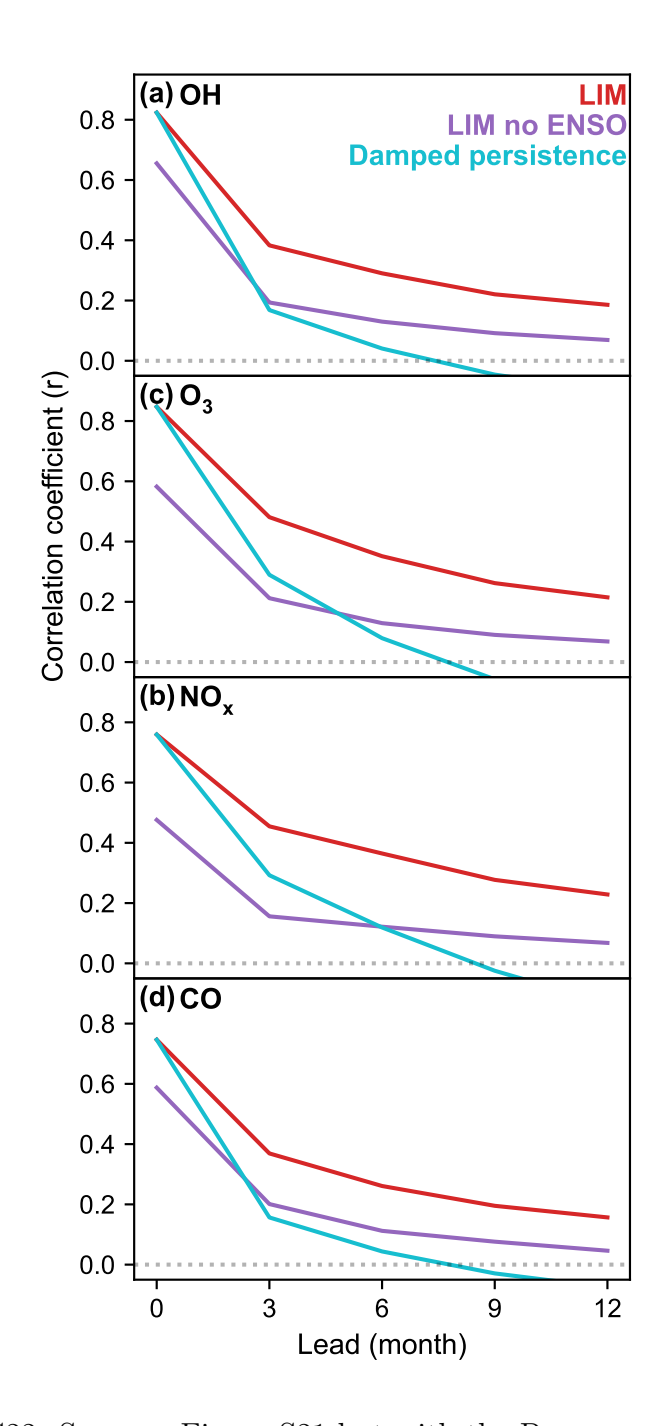


Figure S22: Same as Figure S21 but with the Pearson correlation.

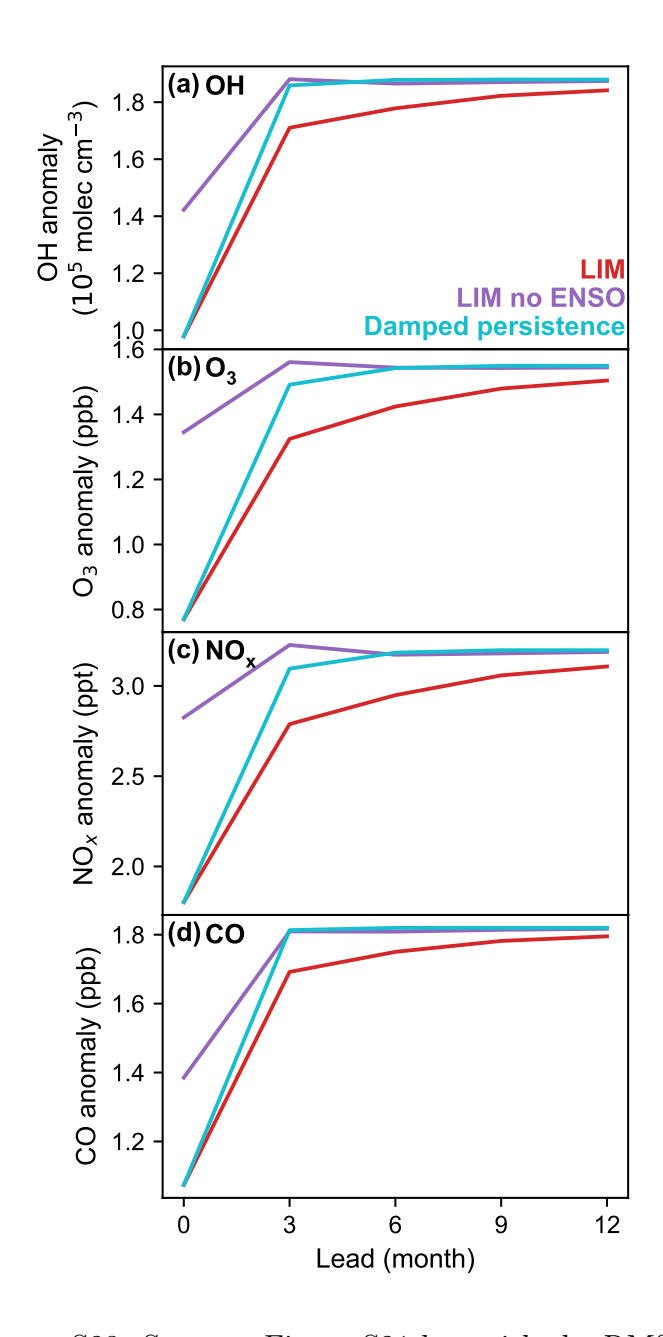


Figure S23: Same as Figure S21 but with the RMSE.

S5 Additional Figures

Figure S24 shows the power spectral density of individual ensemble members of the 300-member 1,000-year LIM simulations compared to the power spectral density of the held-out GFDL-CM3 test set.

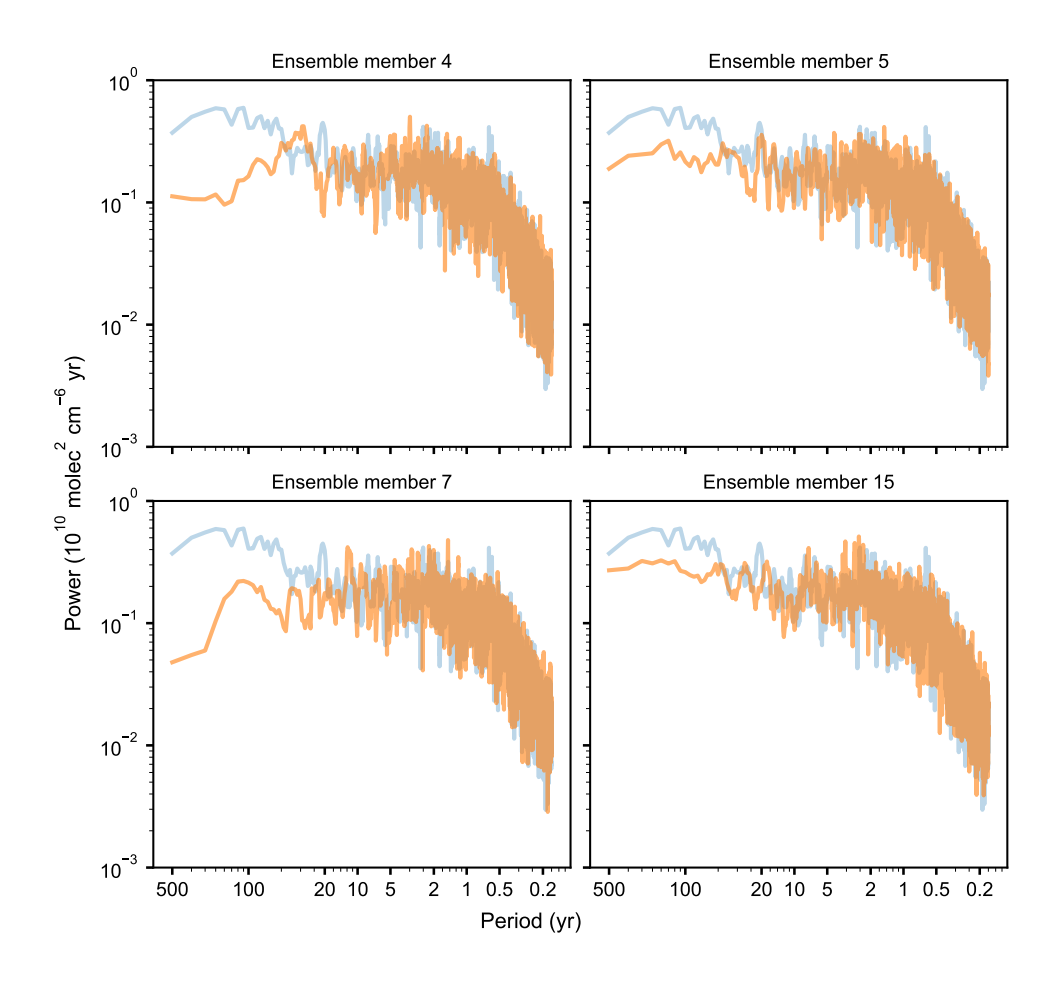


Figure S24: Power spectral density of individual LIM ensemble members (orange) compared to that of the GFDL-CM3 simulation (blue, same as in Figure 2c in the main text).

Figure S25 shows a lead-lag analysis of ENSO in the held-out 1,000-year GFDL-CM3 test simulation. The Niño 3.4 index was calculated and standardized to unit variance. Then, every variable in each grid cell was regressed with the standardized index. The index was shifted earlier or later to obtain patterns associated with months that lead or lag the peak El Niño event.

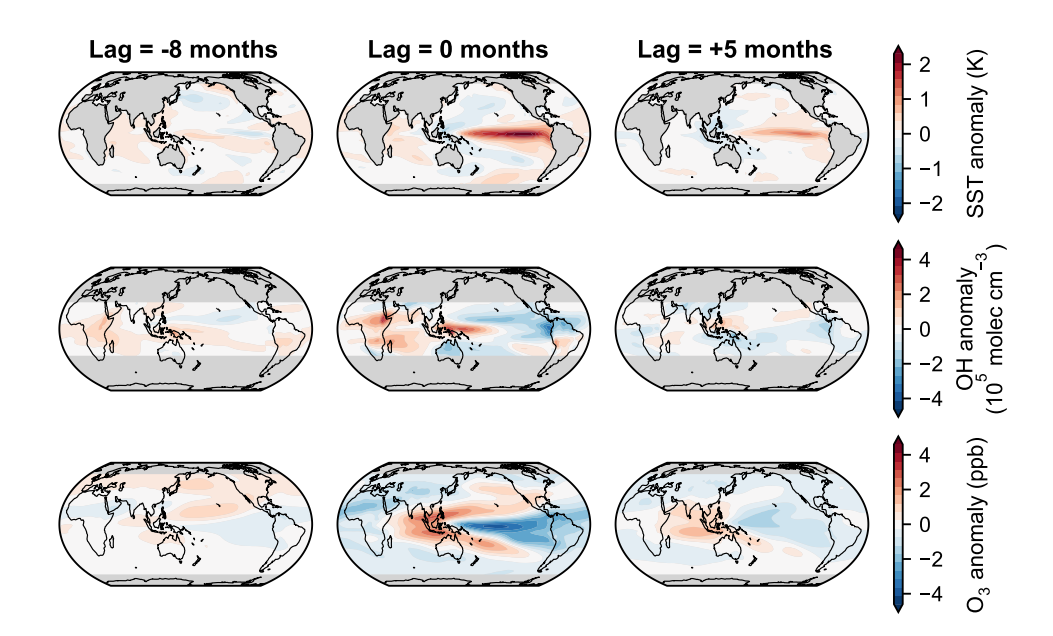


Figure S25: Lead-lag analysis of Niño 3.4 index with SST (top), OH (middle), and ozone (bottom) in the withheld 1,000-year GFDL-CM3 simulation. Columns of the figure show the variables at each grid cell regressed against the Niño 3.4 index shifted 8 months earlier (left), with no time shifting (middle), and shifted 5 months later (right). Patterns are comparable to those in Figure 3 in the main text.

References

Perkins, W. A. and Hakim, G. J.: Coupled Atmosphere–Ocean Reconstruction of the Last Millennium Using Online Data Assimilation, Paleoceanography and Paleoclimatology, 36, e2020PA003959, https://doi.org/10.1029/2020PA003959, 2021.